SATELLITE & MESOMETEOROLOGY RESEARCH PROJECT

Department of the Geophysical Sciences
The University of Chicago

UNPUBLISHED PRELIMINARY DATA

A TECHNIQUE FOR PRECISE ANALYSIS OF SATELLITE DATA

VOLUME II - RADIATION ANALYSIS

by

Tetsuya Fujita

SMRP Research Paper

NUMBER 29

June 1964

MESOMETEOROLOGY PROJECT ---- RESEARCH PAPERS

1.* Report on the Chicago Tornado of March 4, 1961 - Rodger A. Brown and Tetsuya Fujita

2.* Index to the NSSP Surface Network - Tetsuya Fujita

3.* Outline of a Technique for Precise Rectification of Satellite Cloud Photographs - Tetsuya Fujita

4.* Horizontal Structure of Mountain Winds - Henry A. Brown

5.* An Investigation of Developmental Processes of the Wake Depression Through Excess Pressure Analysis of Nocturnal Showers - Joseph L. Goldman

6.* Precipitation in the 1960 Flagstaff Mesometeorological Network - Kenneth A. Styber

7.** On a Method of Single- and Dual-Image Photogrammetry of Panoramic Aerial Photographs - Tetsuya Fujita

8. A Review of Researches on Analytical Mesometeorology - Tetsuya Fujita

9. Meteorological Interpretations of Convective Nephsystems Appearing in TIROS Cloud Photographs - Tetsuya Fujita, Toshimitsu Ushijima, William A. Hass, and George T. Dellert, Jr.

10. Study of the Development of Prefrontal Squall-Systems Using NSSP Network Data - Joseph L. Goldman

11. Analysis of Selected Aircraft Data from NSSP Operation, 1962 - Tetsuya Fujita

12. Study of a Long Condensation Trail Photographed by TIROS I - Toshimitsu Ushijima

13. A Technique for Precise Analysis of Satellite Data; Volume I - Photogrammetry (Published as MSL Report No. 14) - Tetsuya Fujita

14. Investigation of a Summer Jet Stream Using TIROS and Aerological Data - Kozo Ninomiya

15. Outline of a Theory and Examples for Precise Analysis of Satellite Radiation Data - Tetsuya Fujita

* Out of print
** To be published

12151

A TECHNIQUE FOR PRECISE ANALYSIS OF SATELLITE DATA

VOLUME II-RADIATION ANALYSIS

Section 6. Fixed-Position Scanning

by

Tetsuya Fujita

INTRODUCTION

Introduced in Meteorological Satellite Laboratory Report No. 14, Volume I of this work by the author (1963) dealing with techniques for the analysis of satellite data, is a method for the precise photogrammetric analysis of TIROS cloud photographs. Since then the radiation data from medium resolution scanning radiometers aboard TIROS satellites have been investigated intensively, making it possible to devise an accurate method for the evaluation and analysis of the data now available in various forms. This method, developed by the author in cooperation with the National Aeronautics and Space Administration and the Meteorological Satellite Laboratory, U.S. Weather Bureau, is rather general and particularly applicable to researches dealing with Grid Print Radiation Maps, Final Meteorological Radiation Tape Listings, and Radiation Analog Traces from Master Telemetry Tapes.

This text, subdivided into six sections, covers basic problems in constructing infrared maps of terrestrial objects such as clouds and ocean and land surfaces: (1) the solution of fixed-position scanning carried out by fixing the satellite position in space; then (2) its extension to scanning from earth orbiting satellites which are either earth or space oriented; (3) a discussion of terrestrial scan lines leading to computations of the scan vectors and the irradiance vectors of solar radiation for a better understanding of the directional characteristics of terrestrial radiation within the spectral ranges of scanning radiometers; (4) an examination of the spatial response of infrared sensors in connection with the resolution of sensors; (5) the application of the basic knowledge thus introduced to the use of radiation analog traces from which the highest accuracy in infrared mapping and interpretation is expected; (6) a conclusion with a method of interpreting the Final Meteorological Radiation Tape Listings and the Grid Print Maps produced through IBM 7090 computers. These six sections are being presented in several research papers of the Satellite and Mesometeorology Research Project; they will then be combined into a Meteorological Satellite Laboratory Report entitled Techniques for Precise Analysis of Satellite Data; Volume II- Radiation Analysis.

Excluded in this report are the actual examples of meteorological interpretations which by themselves are subjects of great importance in satellite meteorology. Extensive researches on radiation-data interpretation together with photogrammetric interpretation of atmospheric phenomena are now being carried out in Chicago; the results will be published at later dates.

Since the conference on a glossary for satellite meteorology, held at the Meteorological Satellite Laboratory 12 September 1962, the necessity of introducing more terms arose in various phases of research and development. The second conference on the glossary, especially for satellite radiation data analysis, was held at the National Aeronautics and Space Administration 16 December 1963; participants were William R. Bandeen (NASA), William Bonner (U. of Chicago), Tetsuya Fujita (U. of Chicago), Linwood F. Whitney, Jr. (MSL), P. Krishna Rao (MSL), James E. Arnold (U. of Chicago),

and Günther Warnecke (NASA). The glossary which was adopted will appear at the end of Volume II.

As will be seen in this report, the method was so developed that it will result in a resolution limited only by that of the sensor and telemetric system. Nevertheless, the resolution is quite inferior to that of photographs, especially when the radiometer axis points at a considerable slant range.

It has been a difficult problem to analyze data from a closed mode scanning in which a sensor scans terrestrial objects along a helical scan-point track of numerous loops. Difficulties involved in mapping closed-mode data have now been solved, thus making it possible to obtain dual maps over the same area covered by a closed-mode scanning. The time and effort required to obtain these maps have been reduced to no more than would be needed for an open-mode data analysis.

When the scattering angle of the sunbeam is very high a sensor depicts an extremely high specular reflection mixed with outer space contamination. Since this method is designed also to interpret scanning problems under high scan nadir angles, phenomena taking place near the apparent horizon can be investigated from various angles.

6. FIXED-POSITION SCANNING

The axis of a satellite-borne radiometer is firmly attached to a rotating axis, which may be the spin axis of the satellite itself or a separate axis driven by a motor. Such an axis, which provides the scanning motion of a radiometer, is called the scan axis. The angle between the scan axis and the radiometer axis, which is called the inclination of radiometer axis (β), denotes the half-vertex angle of the cone formed by the radiometer axis as it rotates around the scan axis. As shown schematically in figure 77, a conical scan, occurring when $\beta < 90$ deg, changes into a plane scanning in a special case when $\beta = 90$ deg. No attempt, so far, was made to attach two radiometers on one scan axis as illustrated in the figure. TIROS II, III, IV, and VII performed the conical scanning with $\beta = 45$ deg, and the future NIMBUS will have a plane scanning device. The scan cone and the scan plane are thus also defined.

In order to avoid complications resulting from the orbital motion of the satellite, it is first assumed that the satellite remains fixed in space while the radiometer axis completes one revolution around its scan axis. In fact, a satellite travels over 30 miles during the few seconds of the scanning period. It is necessary to assume instantaneous scanning in order to obtain ideal conical or plane scannings. The scan lines thus created are called the instantaneous scan lines.

The nadir angle of the scan axis (η_a), the scan-axis nadir angle, is defined as the angle between the positive direction of the scan axis and the local vertical through the satellite. The positive direction of the scan axis points toward the opening of the scan cone of the specific sensor. In the case of a spin-stabilized vehicle such as the TIROS meteorological satellite, the vehicle's spin axis coincides with the scan axis, thus the nadir angle of the satellite's spin axis, called the satellite nadir angle (η_s), is identical to the scan-axis nadir angle (η_a) of one of the sensors. An earth-oriented vehicle, such as the NIMBUS satellite, for instance, is designed to maintain its η_a as close as possible to 90 deg so that the scan geometry becomes quite simple.

A. SCAN HORIZONTAL ANGLE AND SCAN NADIR ANGLE

The position of a scan point viewed at any instance from a satellite can be expressed by its scan nadir angle (η_*), the nadir angle of the radiometer axis, and the scan horizontal angle (ψ_*), the horizontal angle between two local vertical planes including the scan axis and the radiometer axis, respectively.

Figure 78 reveals the geometry required to compute the scan nadir and scan horizontal angles for a conical scan characterized by the inclination of the radiometer axis (β) and the scan-axis nadir angle (η_a). So in the case of TIROS scanning radiometers, where the vehicle's spinning motion is used as the scanning mechanism of the radiometer, the basic geometry and the solution remain unchanged if we substitute η_a by η_s and the radiometer scan angle (σ) by the TIROS spin angle (μ). The definitions

of both σ and μ appear later; however, they are the rotation angles of either scan or spin axis measured from a reference direction.

During one complete scan, the radiometer axis crosses the scan-axis primary plane twice with maximum and minimum scan nadir angles. The points scanned with these maximum and minimum scan nadir angles are termed aponadir (AN) and perinadir (PN), respectively. It should be noted that there is a pair, aponadir and pernadir for each scan of a radiometer, but they may not always exist on the earth. The scan angle of a radiometer (σ), unless otherwise indicated, is measured in the direction of the scan from the sensor's primary-plane crossing at the aponadir. A primary plane is defined as that which includes a specific axis and the local vertical through the satellite. The term designating the axis is added whenever necessary. The primary line and primary point, as introduced in Volume I of this report, are also generalized in order to apply them to axes other than the TIROS spin axis. Examples are:

AXES	PRIMARY PLANES	PRIMARY LINES	PRIMARY POINTS
spin	spin-axis primary plane	spin primary line	PMs
scan	scan-axis primary plane	scan primary line	PMa
pitch	pitch-axis primary plane	pitch primary line	PMp
roll	roll-axis primary plane	roll primary line	PMr
yaw	yaw-axis primary plane	yaw primary line	PMy
(optical)	(optical-axis primary plane)	(optical primary line)	PMo
optical	principal plane	principal line	PP

The optical axis is an exception since the terms, principal plane, principal line, and principal point have long been used in aerial photogrammetry.

The nadir angles of these axes are designated also by adding the name of each axis, thus scan-axis nadir angle, yaw-axis nadir angle, etc., except where we use the satellite nadir angle for the spin-axis nadir angle and the tilt for the optical-axis nadir angle.

The primary line is defined as the intersection of the primary plane with the image (image primary line) or with the earth (terrestrial primary line). Another line that is extremely useful in analyzing TIROS data with very low minimum nadir angles, and also NIMBUS data, is the secondary line that is perpendicular to the primary line. The positive directions of the primary and secondary lines are taken, respectively, toward those of zero-degree and ninety-degree horizontal angles.

A simple solution of the scan horizontal angle and the scan nadir angle is obtained by solving a spherical triangle on a unit-radius sphere centered at the satellite.

The positive direction of the spin axis penetrates this sphere at the scan-axis primary point (UPMa). The prefix "U" designates the point on a unit-radius sphere. The locus of the scan point (USC) on the sphere keeps a constant great circle distance β from the UPMa thus forming a small circle on the sphere. At the moment when the scan angle is σ, with the scan-axis nadir angle (η_a) and the scan nadir angle ($\eta_{\bullet}$), the great circle distance between USP and USC is obtained as

$$\cos \eta_{\bullet} = \cos \beta \cos \eta_a - \sin \beta \sin \eta_a \cos \sigma \tag{90}$$

where β denotes the inclination of radiometer axis. The scan horizontal angle ($\psi_{\bullet}$) is expressed by either

$$\cos \psi_{\bullet} = \frac{\cos \beta - \cos \eta_a \cos \eta_{\bullet}}{\sin \eta_a \sin \eta} \tag{91}$$

or

$$\sin \psi_{\bullet} = \frac{\sin \beta \sin \sigma}{\sin \eta_{\bullet}} \ . \tag{92}$$

These equations permit us to compute the scan horizontal angle and scan nadir angle from given values of β, σ, and η_a. For actual computations both σ and η_a are expressed as a function of time while β is a known constant.

B.   GRAPHICAL SOLUTIONS

In addition to the computer solutions of the above equations there are two quick graphical methods which can be performed by using the charts and grids introduced in Volume I of this report.

Radiometer Overlay Method. In order to compute $\eta_{\bullet}$ and $\psi_{\bullet}$, using this graphical method it is necessary to construct radiometer overlay (fig. 79). This overlay includes the image scan line which is a circle of intersection between the image plane and the scan cone formed by the radiometer axis of a specific sensor as it scans around its scan axis. The radius of this circle ($R_{\bullet}$), which will be called the image scan circle, depends on the focal distance of the image (f) and the inclination of radiometer axis (β); this radius is expressed by

$$R_{\bullet} = f \tan \beta \ .$$

The scan angle of an image scan point (ISC) is its tangential angle measured from the image aponadir (IAN) in the direction of the scan. The image scan circle is divided, usually, into 36 equal parts in order to label the scan points by scan angles of 10-degree increments.

In determining $\eta_{\bullet}$ and $\psi_{\bullet}$, the radiometer overlay with proper β is placed on a tilt grid with $\tau = \eta_a$ in such a position that the center of the image scan circle coincides with the principal point (IPP) of the tilt grid, and then the overlay is rotated until the image aponadir (IAN) lines up with the zero-degree spin angle. Since the tilt grids (see Vol. I, p. 20), prepared at one-degree intervals of the tilt, include isolines of both horizontal (ψ) and nadir (η) angles viewed from the satellite, the values of $\psi_{\bullet}$ and $\eta_{\bullet}$, can immediately be read off as a function of the scan angle (σ). Examples of the values for β = 25 deg and 45 deg are presented in Tables XVI and XVII.

η_a \ σ	180	170	160	150	140	130	120	110	100	90	80	70	60	50	40	30	20	10	0
0 (upper)	180	170	160	150	140	130	120	110	100	90	80	70	60	50	40	30	20	10	0
0 (lower)	25	25	25	25	25	25	25	25	25	25	25	25	25	25	25	25	25	25	25
10 (upper)	180	164	149	135	121	109	98	88	79	70	61	53	45	37	30	22	15	7	0
10 (lower)	15	15	16	17	18	20	21	23	25	27	28	30	31	32	33	34	35	35	35
20 (upper)	180	139	114	99	89	80	73	66	60	53	47	41	35	29	24	18	12	6	0
20 (lower)	5	6	9	12	16	19	22	25	28	31	34	37	39	41	42	44	44	45	45
30 (upper)	0	36	53	57	58	56	53	50	47	43	38	34	30	25	20	15	10	5	0
30 (lower)	5	7	10	14	19	23	27	31	35	38	41	45	47	50	52	53	54	55	0
40 (upper)	0	15	27	35	39	40	41	40	38	35	33	29	26	22	18	14	9	4	0
40 (lower)	15	16	18	22	25	29	34	38	42	46	50	53	56	59	61	63	64	65	65
50 (upper)	0	9	18	20	29	32	33	33	33	31	29	27	24	20	17	13			
50 (lower)	25	26	27	30	34	38	42	46	50	54	58	62	65	68	70	72			
60 (upper)	0	7	14	19	23	26	28	29	29	28	27	25							
60 (lower)	35	36	37	40	43	46	50	55	59	63	67	71							
70 (upper)	0	6	11	24	20	23	25	26	27	26									
70 (lower)	45	46	47	49	52	55	59	63	67	72									
80 (upper)	0	5	10	14	18	21	23	24											
80 (lower)	55	55	57	59	62	65	68	72											
90 (upper)	0	4	9	13	16														
90 (lower)	65	65	66	68	71														
100 (upper)	0																		
100 (lower)	75																		

Table XVI   Scan horizontal angle (upper) and scan nadir angle (lower) for the scanning radiometer with β = 25 deg. The values to the nearest 1 deg were obtained by the radiometer overlay method.

η_a \ σ	180	170	160	150	140	130	120	110	100	90	80	70	60	50	40	30	20	10	0
0	180	170	160	150	140	130	120	110	100	90	80	70	60	50	40	30	20	10	0
	45	45	45	45	45	45	45	45	45	45	45	45	45	45	45	45	45	45	45
10	180	168	156	144	132	121	111	100	90	80	71	61	52	43	34	26	17	8	0
	35	35	36	37	38	39	40	42	44	45	47	49	50	52	53	54	54	55	55
20	180	164	148	134	121	109	99	89	80	71	62	54	46	39	31	23	15	8	0
	25	26	27	29	32	35	38	41	45	48	51	54	57	59	61	63	64	65	65
30	180	155	133	117	104	94	85	78	70	63	56	49	42	36	29	21			
	15	16	19	23	28	33	38	42	47	52	56	60	64	67	70	72			
40	180	123	103	92	85	79	73	68	62	57	51	46	40						
	5	8	14	21	27	33	40	45	51	57	63	67	72						
50	0	52	63	67	67	65	63	60	56	52	48	43							
	5	9	15	22	29	36	43	50	56	62	69	74							
60	0	24	40	49	53	54	54	53	51	49	45								
	15	17	22	28	34	41	48	55	62	69	76								
70	0	16	29	37	43	47	48	49	48	46									
	25	26	30	35	41	48	55	62	69	76									
80	0	12	22	31	37	41	44	45	45										
	35	36	39	43	49	55	67	69	76										
90	0	10	19	26	33	37	41	43											
	45	46	48	52	57	63	69	76											
100	0	8	16	24	30	35													
	55	56	58	61	66	71													
110	0	8	15	22	28														
	65	66	67	70	74														
120	0																		
	75																		

Table XVII Scan horizontal angle (upper) and scan nadir angle (lower) for the scanning radiometer with $\beta = 45$ deg. TIROS II, III, IV, and VII carried sensors with this inclination of radiometer axis. The radiometer axis does not intersect the earth's surface when the scan nadir angle is larger than 90 deg less dip. The computation was terminated after reading the first value beyond 70 deg of scan nadir angle.

TEC Overlay Method. The radiometer overlay method is very fast as well as helpful in understanding the movement of the scan point as it circles on the image around the image principal point (IPP). Beyond about 45 deg of β, however, an extremely large image is required in order to include the image scan circle. A generalized graphical method, which would overcome this difficulty, can be devised by using a Transverse Equidistant Cylindrical Projection (TEC) Chart and its overlay (see Vol. I, pp. 41 and 49). Figure 78 indicates that the locus of the scan points on the unit-radius sphere is equivalent to a latitude circle if the UPMa is placed at one of the poles. On the other hand, a TEC chart is an equidistant cylindrical chart obtained by wrapping a plane around the sphere with the projection equator through the north and south poles. It is now evident from figure 80 that the spherical triangle formed by three points, UPMa, USC, and USP is transcribed onto a TEC chart by placing PMa at its pole and SP on the projection equator.

As the inclination of radiometer increases from 0 to 90 deg, the locus of the scan point grows from a tiny circle around the scan-axis primary point (PMa) to a square ABCD, the sides of which are at 90 deg to the PMa. The isolines of the scan angle are, of course, great circles departing longitudinally from the primary point (PMa) as a pole. Above the projection equator in figure 80, the isolines for σ = 210, 240, ... 330 are drawn in for orientation purposes. In the actual TEC chart, as introduced in Volume I, p. 49, the isolines are available at one-degree intervals permitting the determination of scan points at much closer intervals. Also seen in the TEC chart are the isolines of β at one-degree intervals.

After locating the scan points on TEC chart as a function of σ and β, the scan nadir and horizontal angles are measured by placing a TEC overlay with its origin at the subsatellite point (SP) in figure 80. In the measuring position, the projection equators of both the TEC chart and its overlay should coincide, and the distance between the scan-axis primary point and the origin of its overlay should be identical to the scan-axis nadir angle (η_a).

The TEC overlay method can be applied to the computation of $\eta_\bullet$ and $\psi_\bullet$ as a function of three variables (β , σ , and η_a) within their all possible ranges, which are

$$0 \le \beta \le 90, \quad 0 \le \sigma \le 360, \quad \text{and} \quad 0 \le \eta_a \le 180 . \qquad (93)$$

This method undoubtedly has advantages over the radiometer overlay method, especially when β is large. The TIROS-borne sensors do not require, at the present time, computations for β other than 45 deg. Examples in Tables XVIII and XIX, computed for β = 70 and 90 deg, may be used for future satellites with radiometers of high inclinations.

-115-

η_a \ σ	180	170	160	150	140	130	120	110	100	90	80	70	60	50	40	30	20	10	0
0	180	170	160	150	140	130	120	110	100	90	80	70	60	50	40	30	20	10	0
	70	70	70	70	70	70	70	70	70	70	70	70	70	70	70	70	70	70	70
10	180	169	159	148	137	127	117	106	96	86	76								
	60	60	61	61	62	64	65	66	68	70	72								
20	180	168	156	144	133	122	112	102	92	82									
	50	51	52	53	55	58	61	64	67	71									
30	180	166	152	139	127	116	106	97	88	79									
	40	41	42	45	49	53	58	62	67	72									
40	180	162	145	131	119	109	100	92	84	76									
	30	31	34	38	43	49	55	62	68	74									
50	180	154	134	120	109	100	93	87	80	74									
	20	22	26	32	39	46	54	62	69	77									
60	180	136	114	104	96	90	86	81	76										
	10	14	20	29	37	46	54	63	71										
70	180	89	87	85	83	81	79	76	74										
	0	9	19	28	37	47	56	65	74										
80	0	42	60	67	71	72	72	72	71										
	10	14	22	30	40	49	58	68	77										
90	0	25	43	54	60	64	67	68											
	20	22	28	35	44	52	62	71											
100	0	18	33	45	52	58	63	66											
	30	31	36	42	49	57	66	75											
110	0	14	27	38	46	53	59												
	40	41	44	49	56	63	71												
120	0	12	23	33	42	50	57												
	50	51	54	58	63	69	76												
130	0	11	21	30	39	47													
	60	61	63	66	70	76													
140	0	10																	
	70	71																	
150	0																		
	80																		

Table XVIII   The scan horizontal angle (upper) and the scan nadir angle (lower) for β = 70 deg. The TIROS-borne horizon sensor has an inclination of 70 deg so that the sensor points toward the outer space during each scan period.

η_a \ σ	180	170	160	150	140	130	120	110	100	90	80	70	60	50	40
10	180														
	80														
20	180	169	159												
	70	70	71												
30	180	168	157	147	136	126									
	60	61	62	64	67	71									
40	180	167	155	143	133	123	114								
	50	51	53	56	60	65	71								
50	180	165	151	138	128	119	111	104							
	40	41	44	48	54	60	67	74							
60	180	160	144	131	121	113	106	101							
	30	31	35	41	48	56	64	72							
70	180	153	133	121	112	106	101	97							
	20	22	28	35	44	53	62	71							
80	180	139	116	107	102	98	96	94							
	10	14	22	31	41	50	60	70							
90	0	90	90	90	90	90	90	90	90						
	0	10	20	30	40	50	60	70	80						
100	0	41	64	73	78	82	84	86							
	10	14	22	31	41	50	60	70							
110	0	27	47	59	68	74	79	83							
	20	22	28	35	44	53	62	71							
120	0	20	36	49	59	67	74	79							
	30	31	35	41	48	56	64	72							
130	0	15	29	42	52	61	69	76							
	40	41	44	48	54	60	67	74							
140	0	13	25	37	47	57	66								
	50	51	53	56	60	65	71								
150	0	12	23	33	44	54									
	60	61	62	64	67	71									
160	0	11	21												
	70	70	71												
170	0														
	80														

Table XIX Scan horizontal angle (upper) and scan nadir angle (lower) for β = 90 deg. A NIMBUS-borne scanning radiometer will have this inclination and its scan-axis nadir angle (η_a) is designed to maintain approximately 90 deg.

C. TERRESTRIAL SCAN LINES

We have expressed a scan point in terms of its nadir and horizontal angles viewed from the satellite. By adding information about the position and attitude of the satellite, the scan points on the earth are computed as a function of time. At this moment, however, we shall continue to discuss scan points under the assumption that the position of a satellite does not change with time.

To make problems simpler the scan axis is kept within a fixed scan primary plane; then the terrestrial scan lines for different scan-axis nadir angles (η_a) are obtained. One of the map projections convenient for the presentation of such scan lines is a <u>Zenithal Equidistant (ZE) Projection</u> which conserves upon projection the azimuth through the subsatellite point and the subsatellite distance. The isolines of $\eta_\bullet$ and $\psi_\bullet$ on this projection chart are, respectively, concentric circles centered at the terrestrial subsatellite point (TSP) and the radials through the subpoint. Thus the height grid as presented in figure 81 is much simpler when compared with the OEC height grid as discussed in Volume I, p. 43.

With the use of Table XIX, a group of scan lines, at 10-degree intervals of scan-axis nadir angles, was drawn in figure 82. In constructing the scan lines a ZE height grid for 1000-km height was used. Even though the scan lines vary with the satellite height, their basic patterns remain unchanged.

The scan lines are symmetrical about the scan primary line and perpendicular at the intersection. At the apparent horizon the scan lines are parallel to the azimuth lines through the subsatellite point. This is an important feature of the scan lines and can be proved by differentiating Eq. (91) while keeping β and η_a constant. Thus we have

$$\left(\frac{\partial \psi_\bullet}{\partial \eta_\bullet}\right)_{\beta, \eta_a} = \frac{\sin \eta_a \, \cos \eta_\bullet \, \cos \psi_\bullet - \cos \eta_a \, \sin \eta_\bullet}{\sin \eta_a \, \sin \eta_\bullet \, \sin \psi_\bullet} \tag{94}$$

Differentiating the equation, which is obtained by solving the plane triangle formed by connecting the satellite, the scan point, and the center of the earth,

$$(\overline{R} + H) \sin \eta_\bullet = \overline{R} \sin (\eta_\bullet + d_\bullet) , \tag{95}$$

where $d_\bullet$ denotes the subsatellite distance of a scan point, $\overline{R}$, the mean radius of the earth, and H, the satellite height, with respect to $d_\bullet$, we obtain

$$\left(\frac{\partial \eta_\bullet}{\partial d_\bullet}\right)_H = \frac{\overline{R} \cos (\eta_\bullet + d_\bullet)}{(\overline{R} + H) \cos \eta_\bullet - R \cos (\eta_\bullet + d)} . \tag{96}$$

Since the variables, β, η_a, and H are constants in these partial differentiations, we may write

$$\frac{\partial \psi_{\bullet}}{\partial d_{\bullet}} = \frac{\partial \psi_{\bullet}}{\partial \eta_{\bullet}} \frac{\partial \eta_{\bullet}}{\partial d_{\bullet}} = \frac{\overline{R} (\sin \eta_a \cos \eta_{\bullet} \cos \psi_{\bullet} - \cos \eta_a \sin \eta_{\bullet}) \cos (\eta_{\bullet} + d_{\bullet})}{\sin \eta_a \sin \eta_{\bullet} \sin \psi_{\bullet} [(\overline{R} + H) \cos \eta_{\bullet} - R \cos (\eta_{\bullet} + d_{\bullet})]}$$

which is reduced to

$$\frac{\partial \psi_{\bullet}}{\partial d_{\bullet}} = \frac{\overline{R} (\sin \eta_a \sin \delta_H \cos \psi_{\bullet} - \cos \eta_a \cos \delta_H) \cos 90}{(\overline{R} + H) \sin \eta_a \sin \delta_H \cos \delta_H \sin \psi_{\bullet}} \qquad (97)$$

when the scan nadir angle approaches $90 - \delta_H$, where δ_H denotes the dip angle corresponding to the satellite height. Equation (97) can be reduced further to

$$\left(\frac{\partial \psi_{\bullet}}{\partial d_{\bullet}} \right)_{\beta, \eta_a, H} = \frac{\overline{R}}{\overline{R} + H} (\sec \delta_H \cot \psi_{\bullet} - \cot \eta_a \csc \psi_{\bullet}) \cos 90 . \qquad (98)$$

It is seen that a terrestrial scan line approaches the apparent horizon in the direction of the azimuth line connecting TSP with the scan point on the apparent horizon except when

$\eta_a = 0$, scan axis toward the earth's center,

$\eta_a = 180$, the earth not scanned,

$\psi_{\bullet} = 0$ or 180, apparent horizon on the scan primary line.

The inclination of the radiometer axis (β) has nothing to do with the orientation of scan lines at the apparent horizon. However, figures 82, 83, and 84 reveal considerable changes in the shape of scan lines when the inclination (β) is changed from 90 deg to 70 deg and finally to 45 deg.

The isolines of scan angle (σ), when β and H are kept constant, also approach the apparent horizon following the azimuth lines. We first differentiate Eq. (92) keeping σ and β constant, thus

$$\sin \eta_{\bullet} \cos \psi_{\bullet} \left(\frac{\partial \psi_{\bullet}}{\partial \eta_{\bullet}} \right)_{\sigma, \beta} + \sin \psi_{\bullet} \cos \eta_{\bullet} = 0 \qquad (99)$$

or

$$\left(\frac{\partial \psi_{\bullet}}{\partial \eta_{\bullet}} \right)_{\sigma, \beta} = - \tan \psi_{\bullet} \cot \eta_{\bullet} , \qquad (100)$$

meaning that the derivative is symmetric with respect to the scan primary line and the scan secondary line. This can be proved by putting the following relationship into Eq. (100):

$$\tan \psi_{\bullet} = -\tan(-\psi_{\bullet}) = -\tan (180 - \psi_{\bullet}) .$$

The orientation of the isoline of the scan angle (σ) at the apparent horizon, obtained from Eq. (100) and (96), is written as

$$\left(\frac{\partial \psi_{\bullet}}{\partial d_{\bullet}}\right)_{\sigma,\beta,H} = -\frac{R}{R+H} \sec \delta_H \tan \psi_{\bullet} \cos 90 \ . \tag{101}$$

The isolines at the apparent horizon are parallel to the azimuth line just as in the case of the scan lines except for $\psi_{\bullet} = 90$ deg or 270 deg. Figures 82 - 84 give the isolines at 10-degree intervals. As well as their derivatives, the lines are symmetric with respect to the scan primary line and to the azimuth line perpendicular to it.

D. SCANNING ANODES OF A SINGLE SENSOR

The scan nadir angle expressed by Eq. (90) reaches a maximum value when $\sigma = 0$, while keeping β and η_a constant. This maximum scan nadir angle, occurring at the aponadir of each scan, is given by

$$\cos \eta^{AN} = \cos \eta_a \cos \beta - \sin \eta_a \sin \beta \tag{102}$$

or $$\eta^{AN} = \eta_a + \beta \ ,$$

where η^{AN} denotes the scan nadir angle at the aponadir.

When the scan angle is 180 deg, Eq. (90), which is reduced to

$$\cos \eta^{PN} = \cos \eta_a \cos \beta + \sin \eta_a \sin \beta \ ,$$

results in two solutions, namely,

$$\eta^{PN} = \eta_a - \beta \ , \quad \text{(outside perinadir)}, \tag{103}$$

when the center of the earth is located outside the scan cone of a specific sensor; and

$$\eta^{PN} = \beta - \eta_a \ , \quad \text{(inside perinadir)}, \tag{104}$$

if the center of the earth is included inside the scan cone.

In the special case where the scan-axis nadir angle is identical to the inclination of radiometer axis, we have

$$\eta^{PN} = \beta - \eta_a = 0 \ . \tag{105}$$

That is to say the radiometer axis at the perinadir orients toward the subsatellite point at the moment of the scan. This point is called the <u>vertical scan point</u> (VS).

A graphical representation of the nadir angles at both aponadir and perinadir can be made on the coordinates, scan nadir angle ($\eta_{\bullet}$) vs scan-axis nadir angle (η_a). An

example of such a diagram which may be called a Scanning Mode Nomogram is presented in figure 85. As Eq. (102) reveals, the isolines of β, representing the aponadirs, are the straight lines originating at the left half of the top of the nomogram and running toward the lower left with 45-degree tilt. Upon reaching the left end of the nomogram these lines reflect toward the lower right, designating the nadir angles of the inside perinadirs. After reflecting again at the bottom of the nomogram, the lines of β-constant represent the nadir angles of the perinadirs when they terminate at the right half of the nomogram top.

It is important to note that the isolines of a specific β, representing the apona-dirs as well as the inside and outside perinadirs, can be traced by way of two 90-degree kinks taking place at the left and the bottom of the nomogram. The area bounded by these three straight lines of β-constant and the top of the nomogram denotes the range of the nadir angle scanned by a sensor with β. Since the upper limit of the scan nadir angle is the function of the satellite height, a group of horizontal lines indicating the upper limit $(90 - \delta_H)$ viewed from various altitudes were added to the nomogram. Thus the ranges of the nadir angles as a function of β, η_a, and H can be determined with the nomogram immediately.

Presented in figure 86 is the range of the nadir angles scanned by a sensor with β = 45 deg, the inclination of TIROS II, III, IV, and VII scanning radiometers. The range is obtained by tracing the straight lines of β = 45 deg. The line AD at the top is the horizon viewed from the sea level. The apparent horizon (EF) from 700 km, aver-age TIROS I height shown by a broken horizontal line, indicates the upper limit of the earth-viewing nadir angle from this altitude. The actual range in which terrestrial objects are scanned is thus included inside the area EBCF.

Scanning Mode of Single Sensor. It has been shown in the previous discussions that a terrestrial scan line either forms a closed loop or ends at the apparent horizon resulting in a horse-shoe like curve. The scanning modes corresponding to these scan lines are termed the closed mode and the open mode, respectively, by Bandeen (1962) who investigated the scan geometry of TIROS II infrared radiometers. The closed mode is loosely called the downward mode, but the fact that a scan axis points downward does not always result in a closed-mode scanning. No scan will take place in a down-ward mode if the satellite altitude is too high for a given β.

The scanning mode nomogram of TIROS from the 700-km altitude shown in figure 86 reveals that the terrestrial scan lines end at the apparent horizon when the scan-axis nadir angle (η_a) lies between points E and F, thus forming an open mode. At the point E the range of scan nadir angles does not extend beyond the apparent horizon, but fluctuates between E and G. For the scan-axis nadir angle smaller than that of EG, the entire range of nadir angles between the aponadir and perinadir stays below the appar-ent horizon, and terrestrial scan lines form loops.

For further generalization of scanning mode problems, the TIROS altitude at 700 km is gradually increased so that the apparent horizon lowers to that of B. By

doing this the region of the closed mode diminishes to zero at the 2600-km altitude and $\eta_a = 0$, (B) at which the scan cone makes tangential contact with the earth at the apparent horizon as viewed from the satellite. If the height of the satellite is further increased, the apparent horizon becomes lower than that of B, thus the earth's surface cannot be scanned until the apparent horizon meets the inside perinadir line at H. From H to I the scanning mode is undoubtedly an open mode since all scan lines end at the apparent horizon.

In addition to the closed and open mode scannings, a third mode called the null mode should be considered; here the axis of a radiometer does not intersect the earth during the scan period. A sensor in its null mode simply means that it does not scan the earth's surface. There is the possibility that the sun, the moon, and other heavenly bodies are scanned and detected. The null-mode scanning takes place when the apparent horizon lies to the left of the inside perinadir line (BC) or to the right of the outside perinadir line (CD). In the former case the center of the earth is found inside the scan cone, and in the latter outside. The null mode corresponding to these cases may be subdivided into the inside null mode and the outside null mode, according to the position of the center of the earth which will be found either inside or outside the scan cone.

The scanning modes of a specific sensor are thus summarized as:

1. Closed Mode - A scanning mode in which a terrestrial scan line forms a closed loop;

2. Open Mode - A scanning mode in which terrestrial scan line ends at the apparent horizon;

3. Null Mode - A scanning mode in which no terrestrial scan line exists when the center of the earth is located inside (Inside Null Mode) or outside (Outside Null Mode) the scan cone.
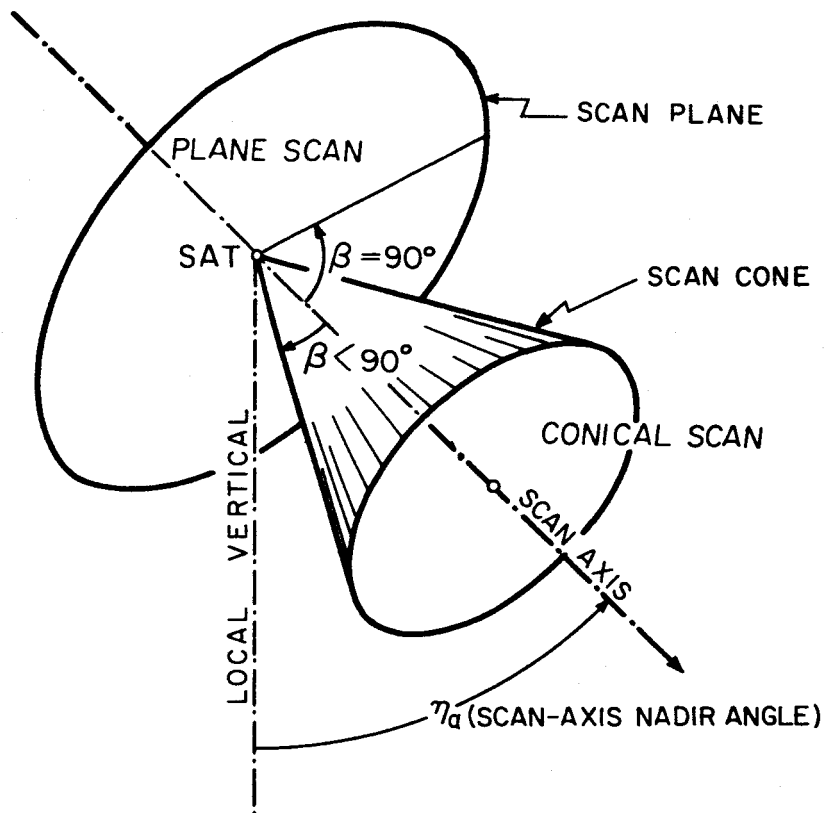
Figure 77. Definition of the conical and plane scans created by rotating the radiometer axis of a specific sensor around the scan axis. The positive direction of the scan axis points toward the opening of the cone. Abbreviations: β (inclination of radiometer axis), η_a (scan-axis nadir angle).
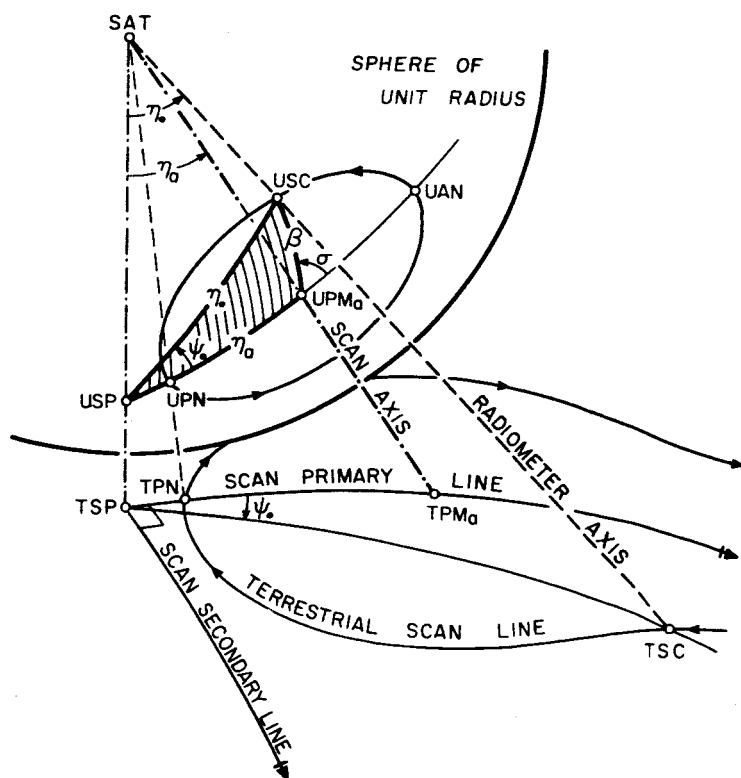
Figure 78. Geometry to compute the scan nadir angle and the scan horizontal angle as a function of the scan angle of the radiometer. The scan primary line denotes the intersection between the scan-axis primary plane and the earth. Its positive direction is chosen to that of zero-degree horizontal angle. Another great circle through the sub-point, oriented toward the 90-degree horizontal angle, is the scan secondary line. Abbreviations: SP (subsatellite point), PN (perinadir), SC (scan point), AN (aponadir), PMa (scan primary point), β (inclination of radiometer axis), η_o (scan nadir angle), ψ_o (scan horizontal angle), η_a (scan-axis nadir angle), σ (scan angle).
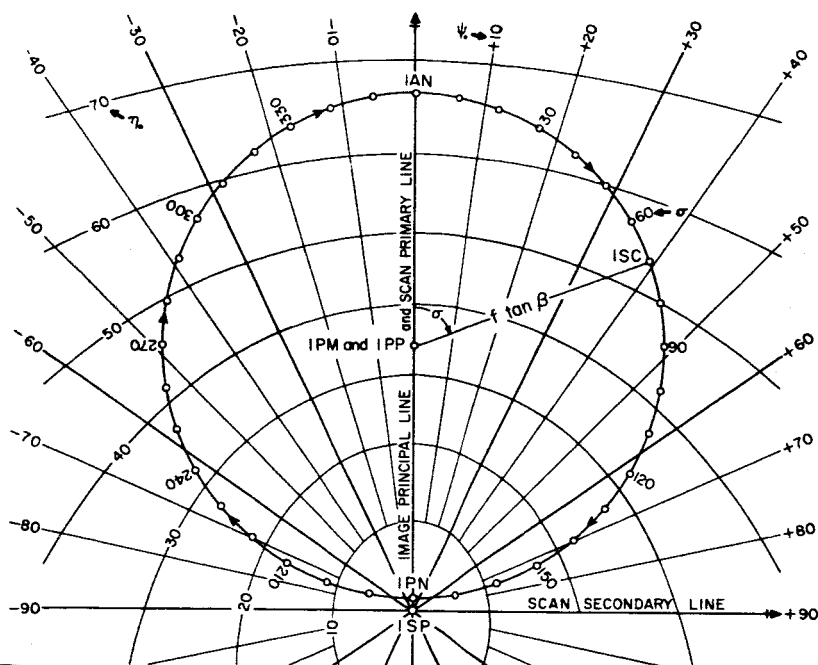
Figure 79. Use of the radiometer overlay method to determine the scan, nadir,and horizontal angles. The isolines of ψ_e and η_e are on the tilt grid and the image scan points on the radiometer overlay. Abbreviations: PM (primary point), PP (principal point), PN (perinadir), AN (aponadir), SP (subpoint), η_e (scan nadir angle), ψ_e (scan horizontal angle), σ (scan angle).
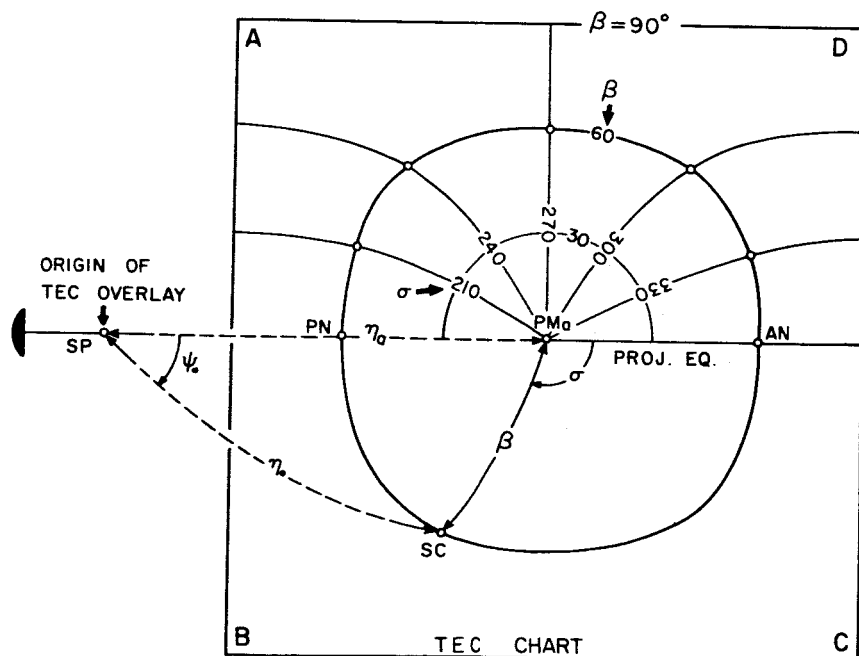
Figure 80. Computation of the scan horizontal and nadir angles using a TEC chart and its overlay. The lines on the TEC overlay are indicated by the dashed lines. Shown above the projection equator are the loci of the scan points for 30, 60,and 90 deg of the inclination of radiometer axis and the isolines of scan angles at 30-deg intervals. Abbreviations: SP (subpoint), PMa (scan primary point), AN (aponadir), PN (perinadir), SC (scan point), β (inclination of radiometer axis), η_e (scan nadir angle), ψ_e (scan horizontal angle).
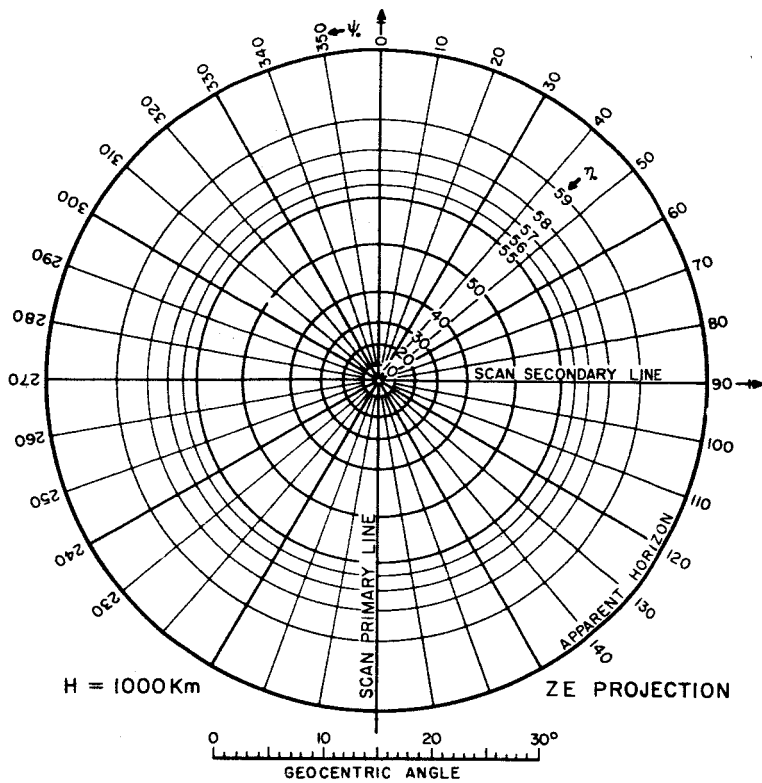
Figure 81. A 1000-km height grid in zenithal equidistant projection including the isolines of the scan horizontal and nadir angles. They are the radials and the circles centered at the subpoint. Abbreviations: ZE (zenithal equidistant), η_s (scan nadir angle), ψ_s (scan horizontal angle).
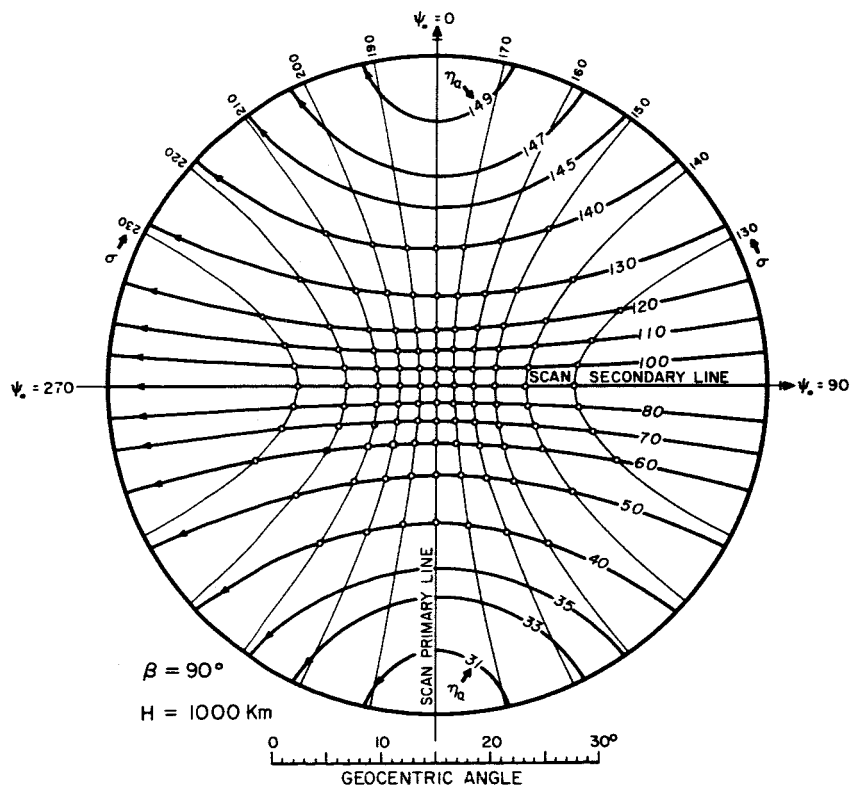
Figure 82. The scan lines (heavy) and the isolines of scan angles at 10-deg intervals drawn on a ZE height grid. The inclination of the radiometer axis is taken as 90 deg, which is the nominal inclination for NIMBUS Satellites. Abbreviations: η_a (scan-axis nadir angle), η_s scan nadir angle), ψ_s (scan horizontal angle), β (inclination of radiometer axis), σ (scan angle).
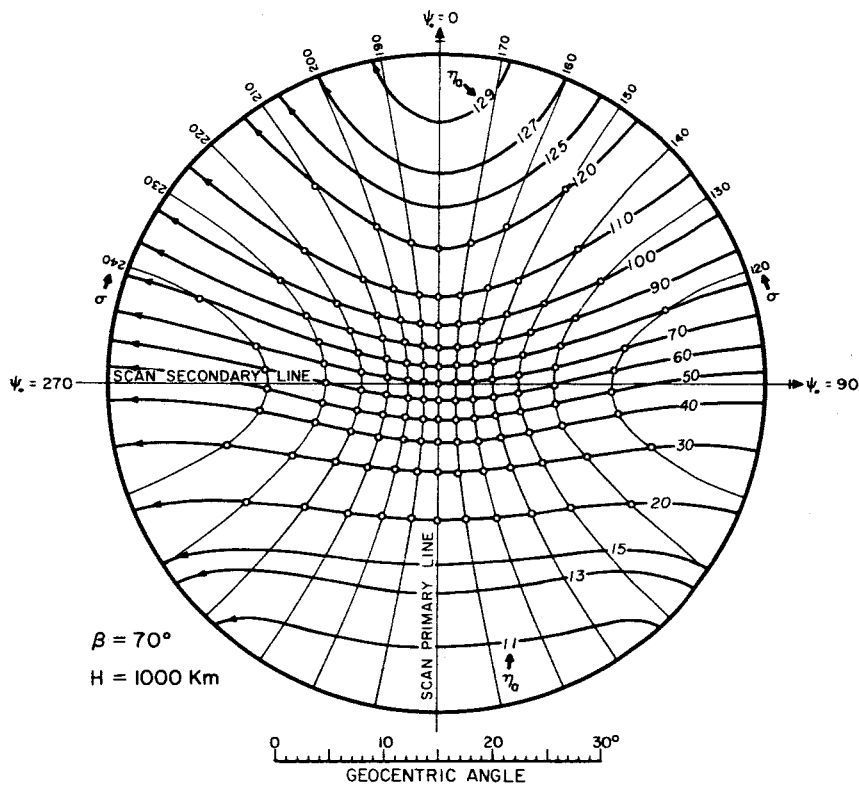
Figure 83. Scan lines and iso-spin-angle lines for scanning with 70 deg of the inclination of radiometer axis. The isolines are drawn on a ZE height grid. This inclination is used for the TIROS horizon sensor in order to obtain space viewed position of the sensor during each scan. Abbreviations: η_a (scan-axis nadir angle), η_o (scan nadir angle), ψ_o (scan horizontal angle), σ (scan angle).

Figure 84. Scan lines and iso-scan-angle lines for scanning with 45 deg of the inclination of radiometer axis. The isolines are drawn on a ZE height grid. TIROS medium resolution radiometers have this inclination. Note that the scan lines form loops on the earth when the nadir angle is lower than 15 deg. Abbreviations: η_a (scan-axis nadir angle), η_o (scan nadir angle), ψ_o (scan horizontal angle), σ (scan angle).
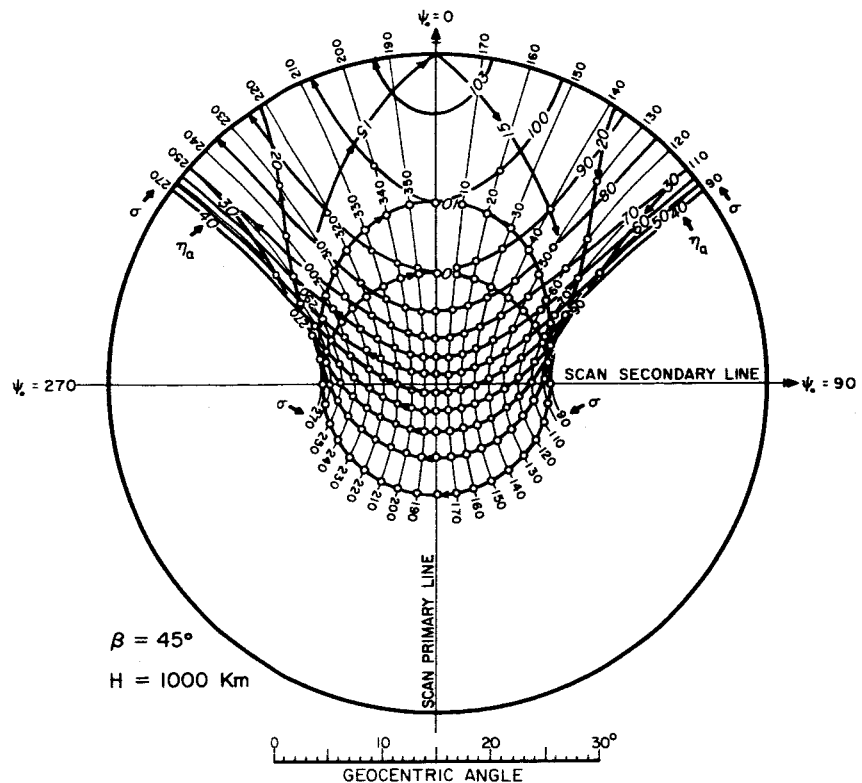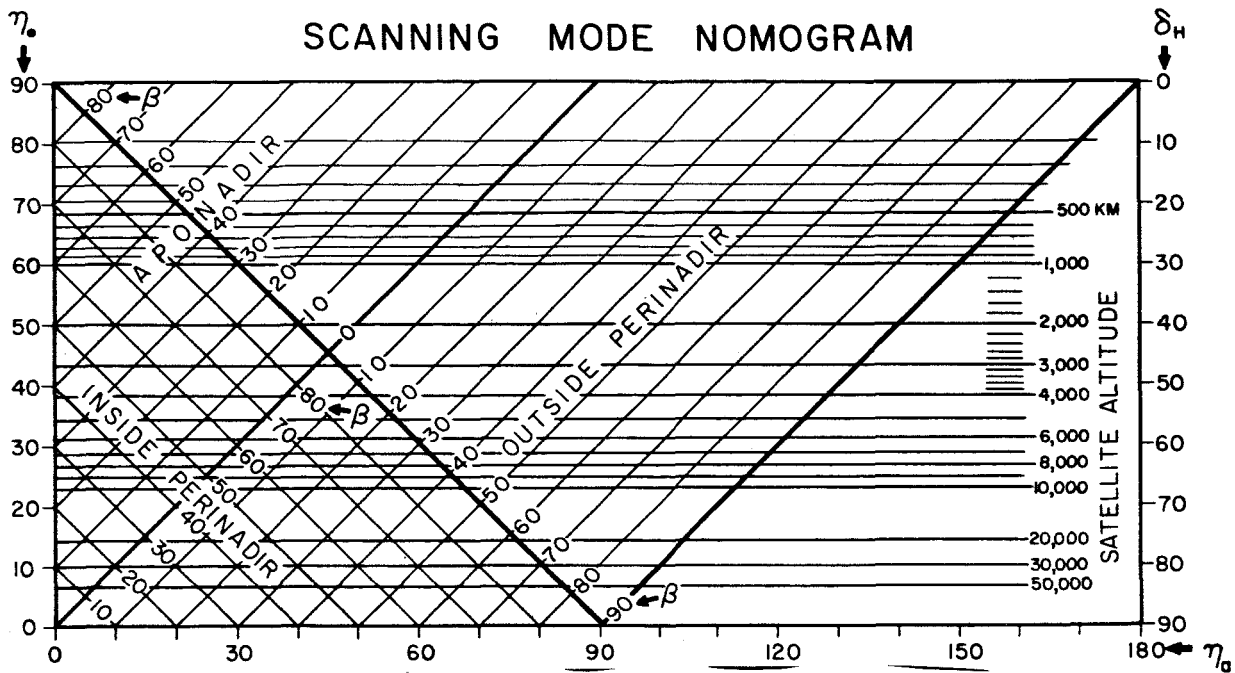
Figure 85. Scanning mode nomogram for a single sensor. The lines with 45-deg tilt represent the aponadir, the inside perinadir, and the outside perinadir for different inclinations of the radiometer axis. Horizontal lines labeled by the height of the satellite indicate the scan nadir angles of the apparent horizons viewed from these heights. Abbreviations: β (inclination of radiometer axis), η_e (scan nadir angle), δ (dip angle), η_a (scan-axis nadir angle).
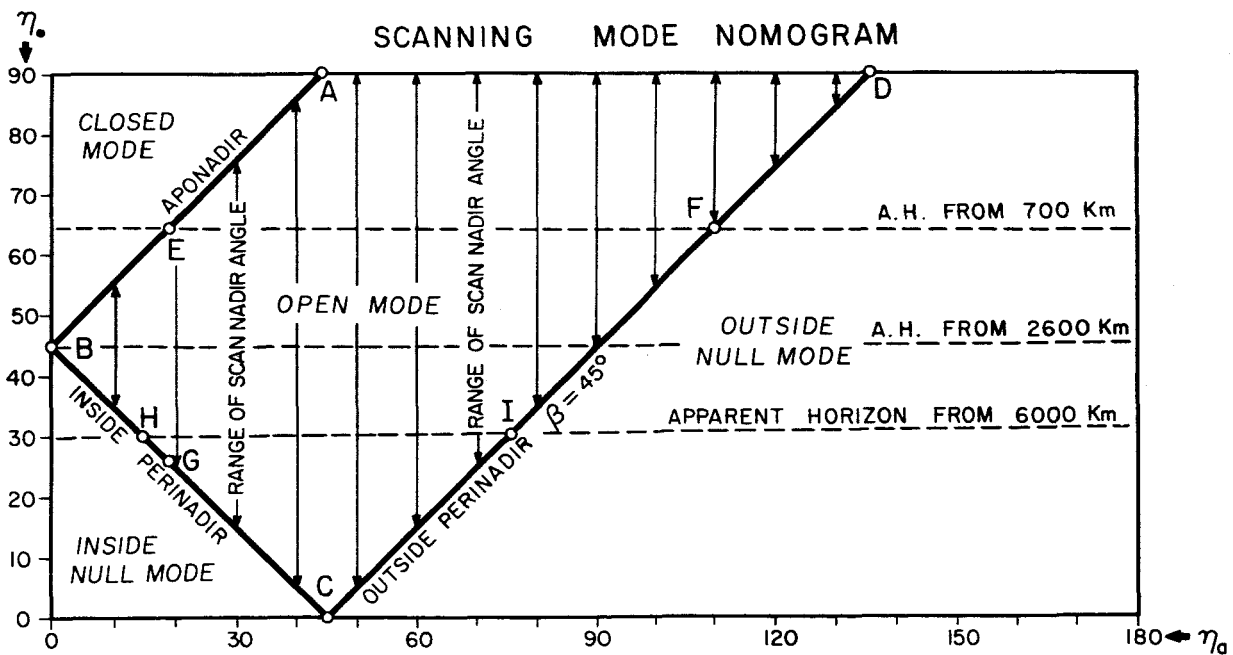
Figure 86. An example of determining the range of the scan angles by using the scanning mode nomogram. The regions of four basic scanning modes of a single sensor are designated as the open mode, the closed mode, the inside null mode, and the outside null mode. Abbreviations: β (inclination of radiometer axis), η_e (scan nadir angle), η_a (scan-axis nadir angle).

MESOMETEOROLOGY PROJECT ----.--- RESEARCH PAPERS

(Continued from front cover)